Raman light scattering and *c*-axis resistivity evidence for a pressure-induced stage transformation in $PdAl_2Cl_8$ intercalated graphite

E. McRae,[1] B. Sundqvist,[2] T. Wagberg,[2] P. Jacobsson,[2,*] R. Vangelisti,[1] and M. Lelaurain[1]
[1]*Laboratoire de Chimie du Solide Minéral, UMR C.N.R.S. 7555, Université Henri Poincaré-Nancy 1, Boîte Postale 239, 54506 Vandoeuvre les Nancy Cedex, France*
[2]*Department of Experimental Physics, Umå University, S-90187 Umå, Sweden*
(Received 30 December 1999; revised manuscript received 7 June 2000)

We have examined several samples of first- to third-stage $PdAl_2Cl_8$-intercalated graphite under hydrostatic pressures up to 1 GPa. In stage-1 highly oriented pyrolytic graphite–(HOPG) and single-crystal-graphite-based materials, the *c*-axis resistivity decreases sharply above a few kilobars; pressure release induces a reversible return to the initial value only in the case of the latter sample. Raman spectra taken *in situ* under pressure on a HOPG-based material show similarly irreversible effects. Analysis of the spectra taken on higher-stage samples leads to the conclusion that hydrostatic pressure beyond a few kilobars increases the density of the intercalate within the graphitic galleries, transforming the initial sample to a higher-stage material. Since there is no loss of intercalate, the overall intercalate-to-host charge transfer remains constant so that the Raman frequency is approximately the same for both first- and second-stage products. This is an unusual situation in which there is thus an *apparent* lack of Raman signature in spite of the stage change.

I. INTRODUCTION

It has been well documented that the intercalation into graphite of most electron acceptors yields graphite-intercalation compounds (GIC's) that are electrically more anisotropic than the host material itself, with values of room-temperature resistivity anisotropy $\rho_c/\rho_a > 10^6$ in a number of cases.[1–3] After synthesis at a few hundred degrees centigrade, cooling any given sample to room temperature leaves the intercalate layers in either a liquidlike (disordered) state or with a two- (2D) or three-dimensional (3D) structure, which can be either incommensurate or commensurate with the host lattice. In the case of many acceptor GIC's, several such phases can coexist even within one single sample. These structures can further evolve as the temperature (T) is lowered or the pressure (p) increased, giving rise to liquid→solid or incommensurate→commensurate transitions. A vast literature exists on the structural changes within the layers of, for instance, the fluoride and chloride GIC's and the associated electrical and magnetic effects. While the underlying reasons are not yet clear, it has been experimentally shown that crystallization of the intercalate layer significantly increases the *c*-axis conductivity $\sigma_c(=1/\rho_c)$, as explicitly shown for the $SbCl_5$ (Refs. 4 and 5) and AsF_5 (Ref. 6) GIC's. In both cases, the *c*-axis conductivity is greater by a factor of 3–4 when the intercalate layer is crystallized rather than ''liquidlike.'' The intercalate layer thus plays an ''active'' role in the *c*-axis conduction process and is not simply a neutral spacer.

The present contribution focuses initially on a relatively new, first-stage compound resulting from the intercalation of $PdAl_2Cl_8$ into HOPG.[7] Previous studies[8] have shown that the electrical resistivity is ''metallic'' within (ρ_a) and perpendicular (ρ_c) to the planes (i.e., $d\rho_{a,c}/dT > 0$). The room-temperature anisotropy (ρ_c/ρ_a) can exceed 5×10^6. The behavior of $\rho_c(T)$ is markedly quadratic, as found in certain highly anisotropic high-temperature cuprate superconductors[9] and at 295 K the ''residual'' component is of the order of 75% of the total value. Of particular interest here is the fact that under pressure the *c*-axis resistance exhibits a sharp decrease centered around 0.4 GPa,[8] dropping to about 10% of its initial value by 1 GPa. 001 x-ray diffraction studies done on the samples before the pressure cycle and then after removal from the pressure cell show that in both cases, the samples are first-stage materials. In an attempt to fully understand the observed behavior, we have extended our analyses to second- and third-stage materials that we have recently successfully synthesized and we have attempted to examine the nature of the resistivity transition using other means.

First-order Raman spectroscopy has proved to be a valuable tool for probing lattice dynamics and charge transfer in GIC's.[10,11] Symmetry arguments for graphite show that two E_{2g} modes are Raman active, an interlayer shear mode around 40 cm^{-1} and an intralayer mode at 1581 cm^{-1}. In GIC's, Raman studies have centered on the effects of charge transfer between intercalate and the bounding or inner graphene layers and the upshift in frequency this provokes in the 1581-cm^{-1} line. Of particular interest here are the ambient-pressure Raman studies on graphite intercalated with the chlorides $FeCl_3$,[12] $AlCl_3$,[13] $SbCl_5$,[14] and $AuCl_3$.[15] While pressure-provoked transitions have been experimentally observed in a number of GIC's, to our knowledge Raman scattering has been used to investigate them in only a small number of cases.[16–18]

In what follows, we will present evidence that the pressure-initiated transitions observed in the $PdAl_2Cl_8$ GIC's can be attributed to intercalate-layer densification. Intercalate-poor regions are formed and a consequent stage change takes place; upon pressure release, the relaxation process is sluggish. This interpretation will be seen to be consistent with both the Raman spectra and the *c*-axis resistance results.

II. EXPERIMENT

Full details on synthesis procedures for the first-stage materials can be found in Ref. 7. Summarized briefly, the chloroaluminate $Pd(AlCl_4)_2$ was presynthesized by heating a mixture of $\frac{1}{3}$ $PdCl_2$ and $\frac{2}{3}$ $AlCl_3$ (molar fractions) until a homogeneous liquid was obtained. Slow cooling led to formation of red needlelike $PdAl_2Cl_8$ crystals. The first-stage compounds were obtained by reacting $PdAl_2Cl_8$ vapor with an excess of chlorine gas (0.5–0.7 atm at 25 °C) using a two-zone Pyrex reactor placed in a two-temperature furnace (300–310 °C; 4 days).[7] To prepare the second- or the third-stage compounds, we heated (320 °C under chlorine gas) a mixture of graphite and chloroaluminate with gravimetric ratios based on the chemical composition $C_{22}PdAl_2Cl_{8.5}$. The graphite used in these studies was highly oriented pyrographite (PGCCL-Carbon Lorraine or ZYB–Union Carbide) in the form of rectangular samples ($15\times2\times0.1\,mm^3$) or 4-mm-diameter disks. (001) x-ray diffraction analyses were done to determine stage fidelity.

Measurements of the *c*-axis resistance of a number of stage-1 samples have been presented elsewhere both as a function of temperature from 4.2 to 295 K and as a function of pressure (at 295 K) up to 1.5 GPa.[8] As to the Raman spectra, in addition to some preliminary data on the first-stage spectra under pressure,[19] we present here a set of spectra on first- to third-stage samples before and after pressure treatment.

The Raman spectra taken as a function of pressure for the first-stage materials were recorded through an increasing, then decreasing pressure cycle between 10^{-4} and 0.83 GPa in a sapphire ball anvil cell[20] using a 180° scattering geometry. The beam from an argon-ion laser (Spectra-Physics 2025) operating at 514.5 nm (50 mW) was focused into the cell held at 295 K. Small pieces of the GIC were cut out from a fresh sample under argon atmosphere in a glove box and transferred into the cell together with a 50/50 pentane isopentane mixture used as a pressure medium. The pressure was measured *in situ* using the ruby pressure scale. A Dilor triple monochromator with 1800-lines/mm holographic grating was used to resolve the backscattered Raman spectrum. Slits were set to give a resolution of 3 cm^{-1}.

The more recent spectra taken on a new set of stage-1 through stage-3 samples were recorded using a Renishaw 1000 grating spectrometer with a charge-coupled device (CCD) detector and a notch filter to remove the Rayleigh line. The power density of the probing laser was about 1 W/cm^2. In this case, the first spectrum was acquired over a 400–3500-cm^{-1} spectral range with the samples inside their Pyrex tubes under argon. These tubes, the pressure cell, and the pentane-isopentane pressure-transmitting medium were then placed inside a glove bag, which was fluxed three times with argon. The tubes were opened and the sample was then removed and placed in the cell filled with the pressure medium. The pressure was increased to 1 GPa at 0.1–0.2 GPa/h with two intermediate 1-h stops, held at 1 GPa for 1 h, then returned to ambient pressure, at a rate of −0.06 GPa/h. The pressure cell was placed within the glove bag, fluxed as above, and the sample removed, dried, and placed within the glass tube. To remove any solvent that might still remain on the sample surface, the tube was pumped to primary vacuum, then sealed, and the spectrum remeasured. At no time during the loading or unloading processes did the sample come in direct contact with ambient atmosphere.

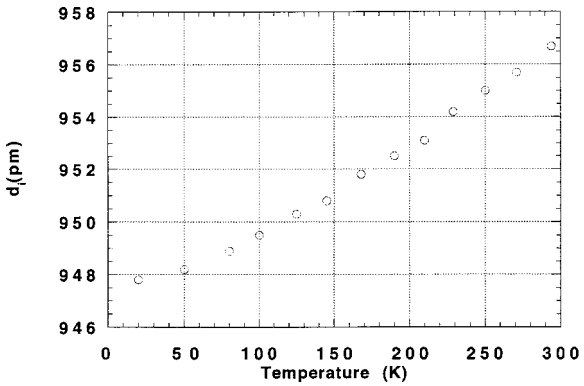

FIG. 1. Thermal variation of interplanar distance d_i for a first-stage HOPG-based sample.

III. RESULTS

The first-stage materials of this study are formulated $C_{22}PdAl_2Cl_{8.5}$. 001 x-ray studies at room temperature and pressure yield an interplanar distance $d_i = 956 \pm 2$ pm. Figure 1 shows a smooth thermal variation, from which the coefficient of thermal expansion (295 K) is determined as $\alpha = [1/d_i(295\,K)](\partial d_i/\partial T) = 40(\pm1)\times10^{-6}\,K^{-1}$. The $(hk0)$ diffractograms of single-crystal-based samples have shown[7] the presence of modulated rings, suggesting some degree of order but only over a very short distance. The graphene stacking is $A/B/A$, where the slash signifies the intercalate layer.

We show in Fig. 2 the results of normalized resistance $[R(p)/R(p=10^{-4}\,GPa)]$ at 292 K for three HOPG-based first-stage samples; designated PdAl-4, -6, and -7, taken, respectively, to 0.7, 1.1, and 1.5 GPa. Marked hysteresis in observed: slow pressure release from the maximum back to ambient pressure leaves the resistance of all three samples at about one-quarter of their initial value. Furthermore, the higher the final pressure a sample has been subjected to, the

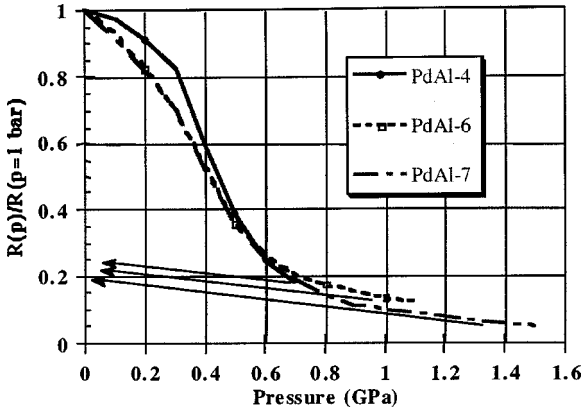

FIG. 2. Variation of the relative *c*-axis resistance, $R_c(p)/R_c$ (10^{-4} GPa=1 bar) as a function of pressure p for three HOPG-based samples, designated PdAl-4, -6, and -7 taken, respectively, to be 0.7, 1.1, and 1.5 GPa. Arrows indicate the final *c*-axis resistance upon p decrease.

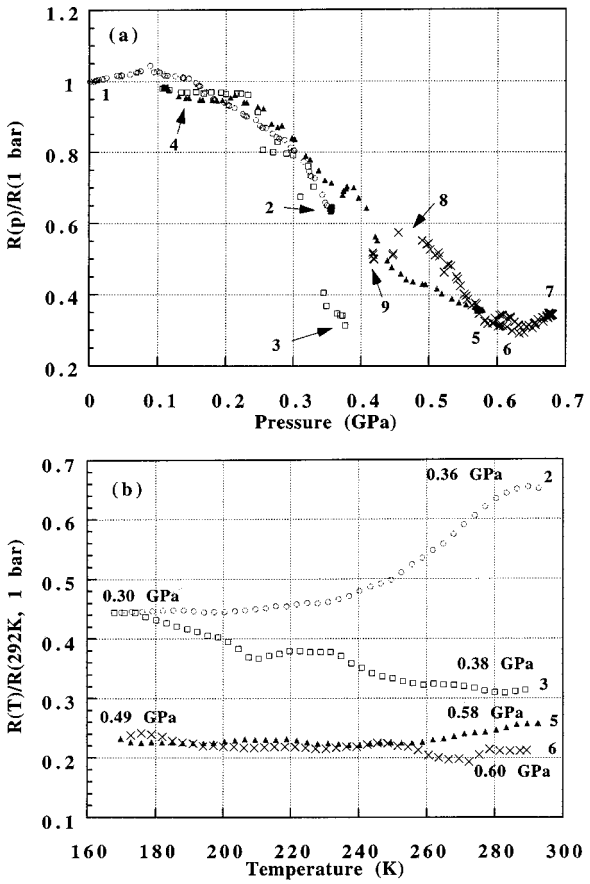

FIG. 3. Series of pressure and temperature treatments applied to the single-crystal-based stage-1 sample. The numbers 1–9 in (a) indicate the sequence, as follows: 1–2; pressure increase at 292 ±2 K; 2 and 3, respectively, the initial and final points of the temperature run [top curves, panel (b)]; 3–4, pressure release at 292 ±2 K; 4–5, pressure increase at 292±2 K; 5 and 6, initial and final points of temperature run [lower curve, panel (b)]; 6–7, pressure increase at 292±2 K, overnight stay at point 7; 7–8, pressure release at 292±2 K over a period of several hours, overnight stay at point 8, to point 9, then returned through the day to point 1. Numbers on right-hand side of (b) show starting and ending points of the temperature runs. The lower curve is downshifted by 0.1 to avoid superposition. The measured pressures at the initial, final, and lowest temperatures (166 K) are indicated in the figure. In both cases, pressure decreased with temperature, and upon reheating to about 290 K, the final pressure was somewhat greater than the initial pressure. The lower curve is almost independent of T and p, contrary to the upper curve taken in the middle of the transition.

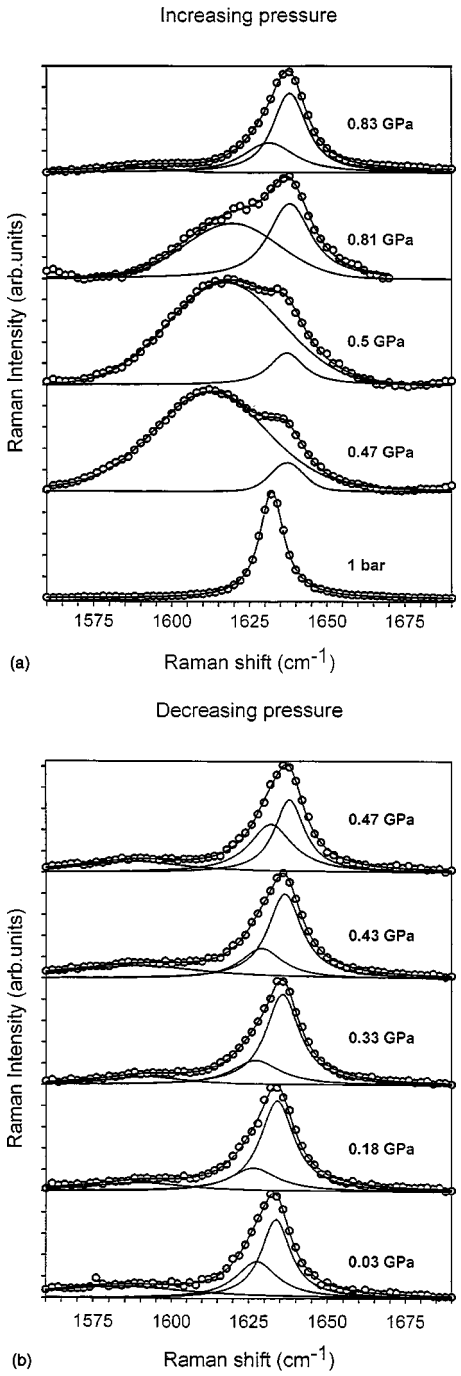

FIG. 4. Raman E_{2g} spectra for (a) increasing and (b) decreasing pressure for a first-stage HOPG-based sample. Circles are experimental data points; lines are results of fits (Table I).

lower the relative *c*-axis resistance after pressure release. The pressure sensitivity, however, is not correlated with the values of $\rho_c(295\,\mathrm{K})$ of the three samples that vary by a factor of 2.

Figure 3 presents a series of results on a single-crystal-based sample. The legend of Fig. 3(a) indicates the sequence of pressure and temperature runs. Contrary to the case of the HOPG-based materials, after pressure release from about 0.7 GPa, the resistance returns to within a few percent of the initial value. The temperature run initiated in the middle of the transition is strongly dependent on T and p. The pressure after the temperature run is marginally higher than the initial pressure, but the relative resistance has decreased from 0.65 to about 0.3. On the other hand, the lower curve of Fig. 3(b) shows much less T and p sensitivity. The transition is not only influenced by thermal effects, as between points 2 and 3, but also there are relaxation effects, as brought out by the small decrease in relative resistance during an overnight stay (points 8–9).

The evolution of the Raman spectrum from 1550 to 1700 cm^{-1} is shown in Fig. 4 for a freshly prepared first stage, HOPG-based sample. As observed for ρ_c (Fig. 2), increasing and decreasing pressure cycles give rise to vastly different modifications of the Raman spectra. The numerical results of the curve analysis illustrated in Fig. 4 are presented in Table I. The initial spectrum and all those analyzed during pressure

TABLE I. Spectral parameters under pressure for a stage-1, HOPG-based sample. ω_1, ω_2, and ω_3 are the center frequencies used for the fits indicated in Fig. 4 with corresponding full widths at half maximum (FWHM) in cm^{-1}.

p (GPa)	ω_1 FWHM % Total area	ω_2 FWHM % Total area	ω_3 FWHM % Total area
10^{-4}	1632.2		
	9.6		
	100 %		
0.47	1637.0	1612.3	
	12.4	44.7	
	5 %	95 %	
0.50	1637.1	1615.8	
	18.1	40.1	
	20.4 %	79.6 %	
0.81	1637.9	1618.2	
	17.3	34.3	
	49 %	51 %	
0.83	1637.4	1626.1	1593.6
	14.5	15.2	22.1
	83.7 %	11.6 %	4.7 %
0.47	1638.0	1632.1	1587.9
	11.7	16.9	43.3
	41.9 %	39.3 %	18.8 %
0.43	1636.5	1629.0	1589.0
	13.2	16.2	39.9
	51.3 %	21.6 %	27.1 %
0.33	1635.8	1627.2	1591.6
	13.1	18.7	32.1
	63.6 %	24.2 %	12.2 %
0.18	1634.4	1627.1	1592.0
	13.0	17.2	31.0
	62.9 %	26 %	11.1 %
0.03	1633.7	1627.6	1582.2
	11.6	16.2	64.0
	44.2 %	27.9 %	27.8 %

release could best be fitted by Lorentzian peaks; those during the pressure increase were somewhat better with Voigt (convoluted Gaussian and Lorentzian peaks). At ambient pressure, the peak is centered at 1632 cm^{-1}, a frequency comparable to that of other first-stage acceptor GIC's. The following spectrum, taken at 0.47 GPa, corresponds, as seen in Fig. 2, to a point within the transition region close to the pressure at which $|d \ln R_c/dp|$ is maximal ($>300\%$ GPa^{-1} at 0.4 GPa). Not only does a very broad second component appear (Table I), but it is dominant and significantly (25 cm^{-1}) downshifted; the initial peak is slightly broadened and is at a slightly higher frequency. As the pressure further rises, Fig. 4 shows that the frequency of the second peak also increases and the full width at half maximum (FWHM) and the intensity decrease. At the maximum applied pressure of 0.83 GPa, the dominant peak is centered at 1637 cm^{-1}, the second at 1626 cm^{-1}, and the FWHM of both are around 15 cm^{-1}. The pressure was then slowly released in steps to 0.03 GPa. The frequency of the highest-frequency component decreased to 1634 cm^{-1}, and the second component was almost

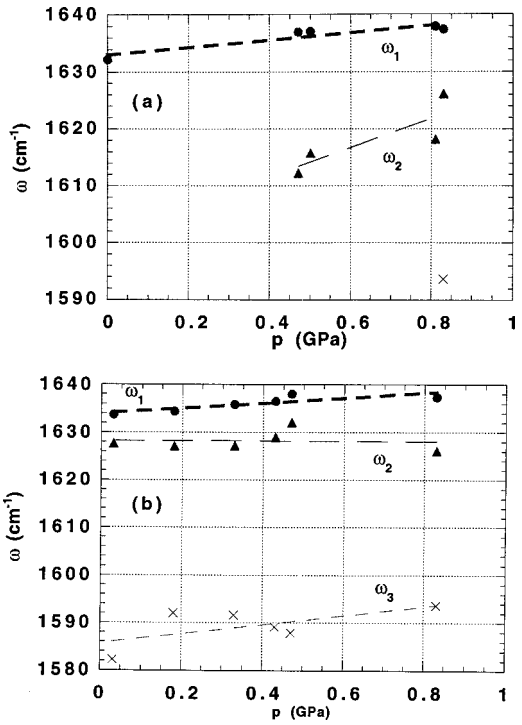

FIG. 5. Variation of Raman frequencies with increasing (top) and decreasing (bottom) pressure.

pressure insensitive: at 0.03 GPa, it was less than 6 cm^{-1} below the upper. These frequency variations with pressure are represented in Fig. 5.

As mentioned in Sec. II, under appropriate conditions, it is possible to synthesize some higher-stage products. We thus studied several freshly prepared samples including a new first-stage compound and two others, identified using x-ray diffraction as being a pure stage-3 material and a mixed stage $1+2$, stage 2 being predominant based on x-ray data. The Raman spectra acquired from 300 to 3500 cm^{-1} before and after a 1-GPa pressure treatment are shown in Fig. 6(a) and over the range around the E_{2g_2} peak in Fig. 6(b). Table II summarizes the important parameters. Fig. 6(a) shows in all cases that there are no significant features below 1500 cm^{-1}; aside from the main peak, there is a wide peak centered around 2700 cm^{-1}, the intensity of which increases after pressure treatment. Figure 6(b) and Table II show that while the original spectra can largely be fitted by a single peak, the spectral decomposition after pressure treatment necessitates a second component or even a third.

IV. DISCUSSION

As the temperature is decreased below 295 K, many GIC's are known to undergo structural transitions, and in several, the application of hydrostatic pressure at ambient temperature can initiate comparable effects. In the case of the GIC's of this study, neither the in-plane (ρ_a) and c-axis (ρ_c) resistivity[8] nor the interplanar distance (Fig. 1) exhibit any detectable anomalous changes upon decreasing T to as low as 4.2 K. On the other hand, the properties of samples subjected to moderate pressures (<1 GPa) change drastically as clearly brought out by Figs. 2–6. The following discussion will center around interpreting these effects. We will first

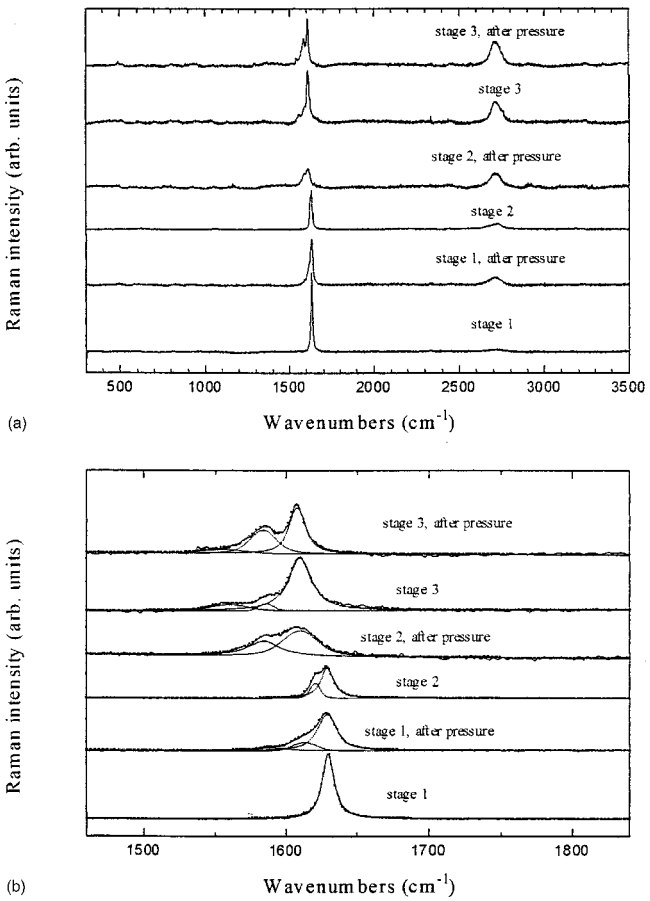

FIG. 6. Spectra for freshly prepared samples, identified by x-ray analysis as being pure stage 1 and 3, and a mixed stage 1 + 2 with stage 2 being predominant. Top panel shows the overall spectra; bottom panel shows the region around the most intense E_{2g} peak. The lower panel shows the spectral decomposition given in Table II.

treat in Sec. IV A the validity of correlating a bulk effect (resistivity) and results of a surface probe (Raman light scattering). Pressure is known to strongly influence structural parameters of GIC's and their effects on electrical properties are dealt with in Sec. IV B. In Sec. IV C we examine the Raman spectra of samples before and after pressure treatment. This analysis leads to hypothesizing in Sec. IV D that Figs. 2–6 can be consistently understood as the result of a pressure-initiated intercalate-layer densification and ensuing stage modification. In Sec. IV E we discuss this interpretation of the *c*-axis resistivity data and finally in Sec. IV F we discuss the strong influence of the host graphite.

A. Can we correlate Raman spectra with bulk resistivity data?

In order to correlate the experimental observations of Figs. 2–4, one might first question whether it is physically meaningful to do so. The *c*-axis resistivity probes bulk-carrier transport through the sample, but the Raman probe depth is very much smaller than the sample thickness; in fact, it has been indicated as varying from about 30 Å (Ref. 21) to several hundred ångstrom (Ref. 22) depending on the value of ρ_c. In view of the high *c*-axis resistivity of our samples, they should thus have a considerable penetration depth compared with many GIC's. Furthermore, the data of Figs. 2 and 3 cannot be simply a sample-dependent surface effect since they are reproducible for samples with different absolute values of $\rho_c(T)$. If the effect detected by the Raman probe was related only to a surface resistance, even an enormous resistance change within this depth could *not* underlie the change observed on Figs. 2 and 3.

That this kind of vibrational spectroscopy is a surface probe but can translate bulk behavior has been confirmed in a number of different instances. Various studies have treated the carbon-layer vibrational modes in chloride-based GIC's as intercalate-poor as 11th-stage $FeCl_3$ in which the *c*-axis repeat distance I_c is about 45 Å: the Raman spectrum quite clearly evolves as the stage index rises from 1 to 11 (Ref. 12) as determined by x-ray diffraction (XRD). Similar evolutions over more limited ranges of stages have been observed in GIC's containing $AlCl_3$ (Ref. 13) and $SbCl_5$ (Ref. 14). For donor GIC's, bulk pressure-induced staging transitions have been followed through Raman scattering[16,23] for a range of samples initially of second stage or poorer. The E_{2g_2} peak position is thus an excellent probe of staging, although as we will see below, it is far more insensitive to ordering within the intercalate layer. One might add that Raman studies on the intercalate layer modes have successfully probed a variety of bulk transitions including, e.g., melting of the intercalate layer[24] in CsC_8 or the order-disorder transition in stage-2 graphite-rubidium.[25]

We believe therefore that the data observed in resistivity and Raman scattering under pressure are due to the same bulk phenomenon. Based on studies done on other GIC's, several possibilities arise, to be examined in the following section.

B. Pressure- and temperature-induced structure modifications and their effects on conduction

Significant drops in ρ_c have been observed in other GIC families, either following application of hydrostatic pressure or lowering of temperature. According to the intercalate and the stage, such significant variations as those observed in Figs. 2 and 3 have been related either to *p*- or *T*-induced (re-)organization of the intercalate layer or to *p*- or *T*-initiated stage changes.

Examining the first possibility, anomalous electrical behavior due to intercalate-layer ordering upon lowering *T* is known for several GIC families.[1,3–6] A Raman-scattering study of the carbon layer modes in the alkali-metal MC_{24} GIC's showed no particular signs upon going through the lower and upper transition temperatures, T_l and T_u, simply the predictable frequency shifts and linewidth modifications.[11,26] Similar studies on rich AsF_5 GIC's showed that the line-shape parameters of the E_{2g_2} mode were insensitive to the onset of ordering in the bounding intercalate layers[27] although ρ_c varies strongly. Based on these results, we are led to conclude that the delocalized electrons in the graphene layers are sensitive to ordering within the intercalate layers since resistive anomalies are observed, but the coupling between the graphene layers and the intercalate is too weak for modifications of the latter to affect the intraplanar E_{2g} phonons. In the case of the heavily studied $SbCl_5$ GIC's, intercalate-layer crystallization can be initiated not

TABLE II. Spectral parameters from Lorentzian peak analyses of Fig. 6. Spectra were taken at room temperature before pressure treatment, then after having been taken slowly to a pressure of 1 GPa and slowly brought back to ambient pressure. The stage-1 sample is different from that of Fig. 4; components 1, 2, and 3 in this table are therefore slightly different than ω_1, ω_2, and ω_3 of Table I. Frequency and FWHM in cm^{-1}. The percentage of total area refers only to first-order peaks.

	First order			Second order
Sample	Component 1 Frequency FWHM % Total area	Component 2 Frequency FWHM % Total area	Component 3 Frequency FWHM % Total area	Component 1 Position FWHM
Stage 1 before pressure	1629.3 10.4 100 %			
Stage 1 after pressure	1628.5 16.9 74.1 %	1612.5 19.5 15.1 %	1587.6 27.2 10.8 %	2706.6 86.8
Stage 2 before pressure	1628.5 11.2 77.4 %	1619.9 8.22 22.6 %		2711.6 88.6
Stage 2 after pressure	1609.4 29.0 61.2 %	1583.7 27.0 38.8 %		2710.9 80.6
Stage 3 before pressure	1609.4 19.4 83.5 %	1585.3 12.6 5.30 %	1559.3 31.5 11.2 %	2716.1 72.1
Stage 3 after pressure	1607.7 13.7 53.2 %	1583.5 22.2 37.9 %	1555.2 36.8 8.94 %	2714.3 73.7

only by lowering the temperature but also by application of pressure[28,29] but we are aware of no Raman study under pressure on this family.

Pressure induced *stage changes* have been observed in both donor- and acceptor-type GIC's. In all but a few cases [$CuCl_2$ and K GIC's (Refs. 30 and 31)], these have dealt exclusively with materials of stage 2 or higher. Using Raman scattering, the staging transitions induced by application of hydrostatic pressure were studied in the alkali-metal[16,23] and $FeCl_3$ GIC's (Ref. 17) for $s \geqslant 2$: the new peak that grew was easily identifiable as being due to creation of an inner graphene layer upon the stage $2 \rightarrow 3$ transformation or its growth in intensity for the stage $3 \rightarrow 4$.

While it is possible for pressure to influence only the intercalate-layer structure without affecting staging, the contrary is not so. In order for a staging transition to take place, there must be a diffusion of the intercalate, creation of more dense regions and movement (or creation) of Daumas-Hérold[32] (DH) walls. Experimental studies on many GIC families have confirmed the strong dependence of ρ_c on stage and intercalate-layer organization, and as we have just discussed, both strongly affect the Raman spectra.

C. Raman spectra before and after pressure treatment

Table III furnishes a number of experimental results concerning the observed Raman frequencies of other stage-1 and

TABLE III. Literature results concerning Raman spectra for stage-1 and -2 GIC's. ω and Γ (in cm^{-1}) are the center frequency and FWHM values.

Intercalate	ω (first stage)	Γ (first stage)	ω (second stage)	Γ (second stage)	Reference
$AlCl_3$	1635.0	3.0	1616.5	4.5	13
$FeCl_3$	1626.0	3.0	1612.9	3.0	12, 21
	1626		1613		17[a]
$AuCl_3$	1627.6	11.6	1617.3	9.2	15
AsF_5	1636.0	5.1			27
	1639.0				22
Sulfate	1632		1616		33
Uranyl sulfate	1632		1616		33
$SbCl_5$			1616 ± 1		14, 27

[a]Study with pressure.

-2 acceptor-type GIC's: the average frequencies are, respectively, 1632.5 ± 6.5 and $1615.4 \pm 2.2\ \mathrm{cm}^{-1}$. We observe that in all cases, the frequency separation is more than adequate to determine unambiguously the stage even taking into account the linewidths and the fact that different samples can yield slightly different values for a given stage and intercalate.

Some of our data were briefly discussed earlier[19] but will be reanalyzed here in the light of new information. The results of our preliminary analysis of the data in Figs. 2 and 4 were somewhat enigmatic inasmuch as the x-ray analyses of all the samples examined both before the pressure runs and after removal from the pressure cell indicated pure stage-1 materials (x-ray studies could not be done *in situ*). Furthermore, this appeared to be in agreement with the Raman peak frequencies at the beginning and at the end of the pressure treatments, which, as observed by comparing Tables I and III, were in the range expected for a stage-1 material. The phenomena observed in Figs. 2 and 4 thus appeared to be representative of materials that were stage 1 both before and after the transition, with perhaps an initially unorganized layer of intercalate transforming into a more organized structure.

It was our intention to investigate more extensively the possibility of such a pressure-initiated in-plane structural change in the intercalate layer through intercalation into a Madagascar single-crystal graphite (SCG) sample so that $(hk0)$ XRD could be carried out after pressure treatment. However, to our surprise, the $\rho_c(p)$ results were those of Fig. 3: in SCG-based samples, the pressure effect on ρ_c was fully reversible. The single-crystal or multidomain structure of the host plays a significant role (cf. Sec. IV F).

As we will now see, based on some newer results and a more complete analysis, we believe that the full interpretation of the experimental results of Figs. 2–4 does indeed involve changes within the intercalate layer, but the major underlying reason is a stage change. Our starting point will be Tables I and II concerning the spectral analyses of Figs. 4 and 6, respectively. Comparison of these tables as concerns the two first-stage samples gives an E_{2g_2} frequency $\omega(s=1) = 1630.3 \pm 2\ \mathrm{cm}^{-1}$. As mentioned above, while XRD showed the ''stage 2'' sample of Fig. 6 to contain only a small amount of stage 1, the Raman results of Table II lead us to suggest that the skin depth ''seen'' by the light scattering probe is essentially stage 1. Indeed, Table II shows that the upper frequency observed ($1628.5\ \mathrm{cm}^{-1}$) is very close to that of the pure stage-1 sample, so we interpret the lower frequency ($1619.9\ \mathrm{cm}^{-1}$) as being the stage-2 component before pressure application. This frequency is a little higher than that of the second component in the stage-1 sample after pressure ($1612.5\ \mathrm{cm}^{-1}$). From these latter two numbers we deduce $\omega(s=2) = 1616.3 \pm 4\ \mathrm{cm}^{-1}$ at ambient pressure. The third-stage sample before pressure treatment has its major peak at $1609.4\ \mathrm{cm}^{-1}$, so we take this to be $\omega(s=3)$ (implying that after pressurization, the stage-2 sample has become essentially stage 3; see below). If we plot these three frequencies versus inverse stage, we obtain a straight line, as observed in other studies: what is even more interesting is that this line is identical to that obtained from a straight line fit to all the previously known acceptor data (cf. Ref. 11, Fig. 2.13). Analyzing the first-order data of Table II further shows that after pressure treatment, all spectra require two or three peaks to fit the experimental data, and the supplementary peaks are always downshifted in frequency. Aside from the E_{2g_2} peak, there are no significant features between 300 and $1500\ \mathrm{cm}^{-1}$ either before or after the pressure treatment.

As to the second-order characteristics, the stage-1 sample (Table II) has no feature around $2700\ \mathrm{cm}^{-1}$ before pressure treatment, whereas there is a small peak for the stage-2 sample, and a much greater and less symmetric peak for the third-stage sample. After pressure treatment, a 2707-cm^{-1} peak appears for the stage-1 GIC and its intensity and frequency increase for the stage-2 and -3 GIC's. This feature in the second-order spectral region in carbonaceous materials is generally associated with structural disorder.[34]

The above analysis of the samples before and after application of hydrostatic pressure leads to the conclusion that such treatment has introduced regions of greater disorder and higher-stage content and that such changes are stable over a period of time. We will examine this idea in the following section concerning the *in situ* study.

D. A pressure-initiated stage transformation?

Figure 4 and Table I summarize the results on the stage-1 GIC, going through the transition. Spectral decomposition is difficult in the case of wide peaks such as those observed during the initial stages of pressurization without *a priori* quantitative knowledge of exactly what is occurring and thus how many peaks should be used in the decomposition. We have used the minimum number consistent with obtaining a good fit to the experimental data and suggest the following interpretation of the spectral decomposition under pressure (Fig. 4 and Table I), taking into account the observed frequencies, surface areas and linewidths (FWHM).

(1) The initial sample is a single-staged material ($s=1$) in which the intercalate layer is not densely packed. This gives rise to the peak at $1632\ \mathrm{cm}^{-1}$, a value typical of that of several first-stage GIC's, as confirmed by Table III.

(2) The first spectrum taken under pressure (0.47 GPa) can be decomposed into a very wide signal (FWHM$\approx 45\ \mathrm{cm}^{-1}$) centered at $1612\ \mathrm{cm}^{-1}$ and a low-intensity, narrow peak at $1637\ \mathrm{cm}^{-1}$. The total surface area of the new peak is $>95\%$ of the total surface area. We interpret this as being due to the fact that application of pressure beyond 0.1 GPa has condensed the intercalate within the galleries, leading to a strongly inhomogeneous, i.e., multistage material with intercalate-depleted and intercalate-densified regions. Such a wide peak is the result of contributions from many locally different stage components, depending on local strain. The total surface area associated with the 1637-cm^{-1} peak being $<5\%$, most of the first stage content has disappeared.

(3) As pressure continues to rise, the upper peak (ω_1) accounts for an increasingly greater percentage of the total peak surface area as its frequency and FWHM slightly rise. We attribute this to formation of a second-stage component in which the intragallery density of intercalate is about twice what it was in the initial first-stage material. This would explain that the frequency is comparable to that of a first-stage material assuming a pressure-independent value of

charge transfer per intercalated entity. As more and more of this dense second-stage GIC is formed, there are increasingly fewer areas of higher-stage content and those that do remain may tend to coalesce, forming richer (lower-stage) areas; thus, the wide peak initially centered at 1612 cm^{-1} rises in frequency rapidly and its contribution to the total peak surface area decreases as it becomes narrower.

(4) By the time the pressure has risen to its highest value (0.83 GPa, Table I), the highest frequency $\omega_1 = 1638\,cm^{-1}$ and the peak associated with the dense second-stage content account for about 85% of total surface area.

(5) Pressure release provokes a few new effects. The FWHM of the two high-frequency peaks ω_1 and ω_2 remain almost constant (cf., Fig. 5) and relatively narrow. ω_1 decreases as would be expected if it were only a pressure effect ($d\omega/dp \approx 5.2\,cm^{-1}$/GPa) while ω_2 remains almost independent of p. The surface areas of these two peaks account for over 80% of the total area throughout the p decrease. It thus appears that the new structure created by the application of pressure is quite stable under pressure release, as translated by both the resistivity and the Raman results upon pressure release (cf. Sec. IV E). A new effect noted is the necessity of a third contribution ω_3 at a much lower frequency, which we interpret as being due to the appearance of some very-high-stage areas, as discussed in Sec. IV C.

As a final comment, Fig. 5 shows that over the pressure range utilized, $d\omega_1/dp = 5.8 \pm 0.6\,cm^{-1}\,GPa^{-1}$ for both increasing and decreasing pressure and the second peak (ω_2) has a similar slope above 0.5 GPa. This value is close to those indicated for the host graphite[10,11,16,35] and agrees well with that observed in first-stage $FeCl_3$ GIC's,[17] which were studied to 5 GPa. In the latter case, no staging transition was indicated for stages 1 and 2 up to 5.18 and 6.61 GPa, respectively, while a reversible transition from stage 3 to stage 4 was inferred at 8.4 GPa.

E. Resistivity and Raman spectra correlation

The light-scattering results yield strong evidence for a pressure-driven change to a higher stage whatever the initial stage. We believe that several features of the $R_c(p,T)$ behavior lend further support to this interpretation, particularly the temperature runs of Fig. 3(b) between 2–3 and 5–6 of Fig. 3(a). Starting at point 2 in the transition zone, as T is decreased, p simultaneously diminishes. A significant decrease in R_c [Fig. 3(b)] is contrary to what would be expected if pressure alone played the dominant role. Increasing T causes p to increase, and R_c further decreases right up to 290 K at which point the pressure is marginally greater than its initial value. This suggests that the initial T decrease and then the subsequent p increase both drive the sample towards formation of the denser second-stage compound. For the temperature-run starting at point 5, R_c is almost independent of p and T. Compared to the lower-pressure results, this can be understood in the light of two factors. First, R_c is much more pressure-sensitive in the middle of the transition zone (point 2) than at 0.6 GPa [cf. Fig. 3(a)]. Second, for almost all known GIC's, ρ_c is less temperature sensitive for a second-stage than for a first-stage GIC.[3] The combined effect gives rise to the almost T- and p-independent behavior of the lower curve on Fig. 3(b). Finally, the value of R_c at points 3, 5, and 6 is the same to within a few percent, suggesting that once the dense stage-2 material has been formed, it is stable over a wide range of pressure.

We believe that such an interpretation is consistent with ideas put forward by Kirczenow. This author presented a model for stage transitions[36] and their kinetics[37] founded on the Daumas-Hérold view of intercalation.[32] Stage disorder was found to be an inherent property. Low-stage numerical calculations showed that the extent of this disorder rose with increasing stage index or temperature and with decreasing domain size, in-plane density or charge transfer, as a result of the competition between the entropy of stage disorder and the energy of repulsion between intercalate layers. On the other hand, it was not expected that the stage disorder would be significantly influenced by other 2D features such as the in-plane intercalate-layer order or registry between intercalate and host. Several results of the preceding paragraph are in line with expectations of this model. First, Kirczenow pointed out[36] the consistency between his model and other experimental results on the temperature driving a mixed stage compound to the lower stage,[38] as discussed above between points 2 and 3 (Fig. 3). Second, strong disorder is suggested by the Raman spectrum taken in the middle of the transition zone (Fig. 4) and this would be consistent with small domain size and low charge transfer associated with acceptor GIC's. Kirczenow pointed out[37] that during stage transitions, the in-plane dimensions of the DH domains could change radically in size and shape, and smaller ones could even appear and disappear. The spectrum taken at 0.47 GPa (Fig. 4) might be proof of this in the case of these GIC's, knowing that Raman spectroscopy is a particularly sensitive probe of domains in carbonaceous materials smaller than those detected using XRD.[34] That pressure treatment has introduced such disorder would further be in line with creation of the second-order features discussed in Sec. IV C. Finally, the slow kinetics during, for example, the overnight stays at a given pressure [e.g., 8–9 on Fig. 3(a)] are further in agreement with the expectations of this staging model.

A final comment is in line as regards the electronic properties of these materials. It has recently been shown using the Shubnikov–de Haas (SdH) effect,[39] that the quantum oscillations in stage-1 $PdAl_2Cl_8$ GIC's can be interpreted within the framework of the strictly 2D Blinowski-Rigaux band model,[40] whereas those of the higher stage-3 materials cannot, suggesting that the latter are less anisotropic. Since in general, the in-plane resistivity of GIC's is relatively insensitive to stage (at least for $s < 10$), this SdH study would suggest lower values of ρ_c as the stage index rises. This is indeed compatible with interpreting Figs. 2 and 3 as a transformation to a higher-stage material under hydrostatic pressure.

F. Role of the host graphite

As illustrated in Figs. 2 and 3, the $\rho_c(p)$ results are a strong function of the host: in SCG samples, the pressure effect on c-axis resistivity was reversible whereas those samples based on HOPG always gave metastable changes. The single-crystal or multidomain structure of the host plays a significant role in the stage transformation. It appears that the domains or domain boundaries initially present within

the HOPG host pin the Daumas-Hérold walls[32] during pressure release, rendering the transition extremely sluggish, whereas this does not occur in the SCG-based material. A host-based difference was also indicated in the pressure-driven stage changes of the alkali-metal GIC's in which the pressure range over which two stages could coexist was greater in SCG-based materials than those synthesized using HOPG. This was attributed to a higher dislocation density in the latter, which facilitated slippage and therefore stage transformation. In $PdAl_2Cl_8$ GIC's on the other hand, the use of HOPG instead of SCG renders the transition irreversible or at least metastable and very sluggish. This would be more in line with the ideas suggested elsewhere that ''domain-wall friction'' or ''viscosity'' might be expected to play a non-negligible role in the kinetics of such transitions.[41]

V. CONCLUSIONS

This study has given evidence of a stage change that is initiated at a pressure lower than that observed for any other first-stage, acceptor-type GIC. What at first appeared to be enigmatic—a single Raman peak at approximately the same frequency both before and after the transformation—can now be fully understood as the result of increasing the density of the intercalate within the galleries upon going from a first- to a second-stage material so that the total charge transfer on each graphene sheet remains approximately the same. All the light-scattering results as well as those concerning the *c*-axis resistance can be qualitatively explained through this mechanism. The transition is found to be broad and very sluggish and we have shown that the nature of the host plays a critical role. A pressure within the cell some 10 times greater than ambient pressure *s* is sufficient to stabilize the second-stage HOPG-based samples: the x-ray studies show that they revert to primarily first stage only after removal from the resistivity cell. It would certainly have been of interest to make further Raman studies by extending the results of Fig. 4(b) below 0.03 GPa. However, it is not an easy task to do so from an experimental viewpoint.

ACKNOWLEDGMENTS

The authors acknowledge financial support from the NFR, TFR, and the Swedish Institute. E. M. received travel support from the French MDRI and the Service des Relations Internationales of U.H.P. P. J. expresses his gratitude to Professor W.B. Daniels at the Department of Physics, University of Delaware, Newark, Delaware for the use of the sapphire ball and anvil cell.

*Present address: Department of Physics, Chalmers University of Technology, S-41296 Göteborg, Sweden.

[1] M. S. Dresselhaus and G. Dresselhaus, Adv. Phys. **30**, 139 (1980).
[2] J. P. Issi, in *Graphite Intercalation Compounds II: Electronic Properties*, Springer Series in Material Science, edited by H. Zabel and S. A. Solin (Springer, Berlin, 1992), Vol. 18, Chap. 6.
[3] E. McRae and J. F. Marêché, J. Mater. Res. **3**, 75 (1988), and references therein.
[4] D. T. Morelli and C. Uher, Phys. Rev. B **27**, 2477 (1983).
[5] O. E. Andersson, B. Sundqvist, E. McRae, J. F. Mareche, and M. Lelaurain, J. Mater. Res. **7**, 2989 (1992).
[6] E. McRae, M. Lelaurain, J. F. Marêché, G. Furdin, A. Hérold and M. Saint Jean, J. Mater. Res. **3**, 97 (1988).
[7] V. Polo and R. Vangelisti, Ann. Chim. (Paris) **19**, 177 (1994).
[8] E. McRae, O. E. Andersson, M. Lelaurain, V. Polo, B. Sundqvist and R. Vangelisti, J. Phys. Chem. Solids **57**, 827 (1996).
[9] S. L. Cooper and K. E. Gray in *Physical Properties of High Temperature Superconductors IV*, edited by D. M. Ginsberg (World Scientific, Singapore, 1994).
[10] S. A. Solin, in *Graphite Intercalation Compounds I: Structure and Dynamics*, Springer Series in Materials Science Vol. 14, edited by H. Zabel and S. A. Solin (Springer, Berlin, 1990), Chap. 5.
[11] M. S. Dresselhaus and G. Dresselhaus, in *Light Scattering in Solids III*, Springer Verlag Topics in Applied Physics Vol. 51 (Springer, Berlin, 1982), Chap. 2.
[12] C. Underhill, S. Y. Leung, G. Dresselhaus, and M. S. Dresselhaus, Solid State Commun. **29**, 769 (1979).
[13] G. M. Gualberto, C. Underhill, S. Y. Leung, and G. Dresselhaus, Phys. Rev. B **21**, 862 (1980).
[14] P. C. Eklund, D. S. Smith, V. R. K. Murthy, and S. Y. Leung, Synth. Met. **2**, 99 (1980).
[15] T. Ishii, M. Nakao, K. Suzuki, T. Enoki, R. Nishitani, and Y. Nishina, Solid State Commun. **84**, 1055 (1992).
[16] N. Wada, Phys. Rev. B **24**, 1065 (1981).
[17] Liu Zhenxian, Wang Lizhong, Zhao Yongnian, Cui Qilang, and Zou Guangtian, J. Phys.: Condens. Matter **2**, 8083 (1990).
[18] S. Matsuzaki, T. Kyoda, T. Ando, and M. Sano, Solid State Commun. **67**, 505 (1988).
[19] P. Jacobsson, E. McRae, B. Sundqvist, R. Vangelisti, and M. Lelaurain, *Extended Abstracts, Carbon '96* (British Carbon Group, Newcastle Upon Tyne, 1996), pp. 122–123.
[20] M. J. Lipp and W. B. Daniels, Phys. Rev. Lett. **67**, 2810 (1991).
[21] N. Caswell and S. A. Solin, Solid State Commun. **27**, 961 (1978).
[22] I. Ohana and Y. Yacoby, Phys. Rev. Lett. **57**, 2572 (1986).
[23] R. Clarke, N. Wada, and S. A. Solin, Phys. Rev. Lett. **44**, 1616 (1980).
[24] N. Caswell and S. A. Solin, Phys. Rev. B **20**, 2551 (1979).
[25] J. Giergiel, P. C. Eklund, R. Al-Jishi, and G. Dresselhaus, Phys. Rev. B **26**, 6881 (1982).
[26] P. C. Eklund, G. Dresselhaus, M. S. Dresselhaus, and J. E. Fischer, Phys. Rev. B **16**, 3330 (1977).
[27] P. C. Eklund, E. R. Falardeau, and J. E. Fischer, Solid State Commun. **32**, 631 (1979).
[28] B. Houser, H. Homma, and R. Clarke, Phys. Rev. B **30**, 4802 (1984).
[29] M. Lelaurain, J. F. Marêché, E. McRae, O. E. Andersson, and B. Sundqvist, J. Mater. Res. **7**, 2276 (1992).
[30] V. A. Nalimova, T. Yu. Sokolova, V. V. Avdeev, and K. N. Semenenko, Mater. Sci. Forum **91–93**, 401 (1992).
[31] C. D. Fuerst, J. E. Fischer, J. D. Axe, J. B. Hastings, and D. B. McWhan, Phys. Rev. Lett. **50**, 357 (1983).
[32] N. Daumas and A. Hérold, C. R. Acad. Sci. Paris **268**, 373 (1969).
[33] A. Moissette, A. Burneau, J. Dubessy, H. Fuzellier, and M. Lelaurain, Carbon **33**, 1223 (1995).
[34] H. Wilhelm, M. Lelaurain, E. McRae, and B. Humbert, J. Appl.

Phys. **84**, 6552 (1998), and refs. therein.
[35] M. Hanfland, H. Beister, and K. Syassen, Phys. Rev. B **39**, 12 598 (1989).
[36] G. Kirczenow, Phys. Rev. Lett. **52**, 437 (1984): Phys. Rev. B **31**, 5376 (1985).
[37] G. Kirczenow, Phys. Rev. Lett. **55**, 2810 (1985).
[38] J. E. Fischer, C. D. Fuerst, and K. C. Woo, Synth. Met. **7**, 1 (1983).
[39] R. T. F. van Schaijk, A. de Visser, E. McRae, and R. Vangelisti (unpublished).
[40] J. Blinowski, Nguyen Hy Hau, C. Rigaux, J. P. Vieren, R. Le Toullec, G. Furdin, A. Hérold, and J. Mélin, J. Phys. (France) **41**, 47 (1980).
[41] H. J. Kim and J. E. Fischer, Phys. Rev. B **33**, 4349 (1986).